Thermochimica Acta 494 (2009) 80–85

Contents lists available at ScienceDirect

Thermochimica Acta

journal homepage: www.elsevier.com/locate/tca

Advanced isoconversional kinetics of nanocrystallization in $Fe_{73.5}Si_{13.5}B_9Nb_3Cu_1$ alloy

Hossein Asghari Shivaee[a], Hamid Reza Madaah Hosseini[b,*]

[a] Institute of Nanoscience and Nanotechnology, Sharif University of Technology, Tehran, Iran
[b] Department of Materials Science and Engineering, Sharif University of Technology, Tehran, 1458889694, Iran

ARTICLE INFO

Article history:
Received 19 January 2009
Received in revised form 25 April 2009
Accepted 27 April 2009
Available online 3 May 2009

Keywords:
Finemet alloy
Nanocrystallization
Isoconversional kinetics
Calorimetery

ABSTRACT

Nanocrystallization kinetics of amorphous Finemet alloy was studied using Vyazovkin advanced isoconversional method under non-isothermal condition. Well known Kissinger model-fitting method and four isoconversional methods of Kissinger–Akahira–Sunose (KSA), Flynn–Wall–Ozawa (FWO), Tang, and Starink were also used for the determination of activation energy. Differential scanning calorimetry (DSC) and X-ray diffraction (XRD) patterns were used for thermal and structural analyses, respectively. According to Vyazovkin and other isoconversional methods, the mean value of variable activation energy, as a function of conversion, was obtained as 350 kJ mol^{-1}. While, according to Kissinger method, the constant value of activation energy was obtained as 270 ± 10 kJ mol^{-1} for the same experiments, which shows inaccuracy of this method. The mean value of kinetic exponent $\langle n \rangle$ was 1.44 ± 0.05 by considering instantaneous nucleation condition ($n = m$), which is consistent with one-dimensional growth mechanism. Kinetics and mechanistic predictions were also performed using numerical reconstruction of the experimental kinetic function. Comparison of the numerically reconstructed model with theoretical ones showed that no single model could perfectly fit the numerical values of kinetic function and the mechanism of transformation changes with conversion progress. Nevertheless it could be seen that nanocrystallization almost follows the one-dimensional diffusion mechanism.

1. Introduction

Nanocrystalline Finemet alloy with the nominal composition of $Fe_{73.5}Si_{13.5}B_9Cu_1Nb_3$ exhibits excellent soft magnetic properties. This Fe–Si–B based alloy with small addition of Cu and Nb is produced as amorphous precursor by melt spinning and subsequent nanocrystallization heat treatment. During the crystallization, first, a magnetically desirable Fe–Si phase appears (main transformation) and then precipitation of boride phases begins to form, which are deleterious to good soft magnetic behavior of the alloy. Appropriate heat treatment leads only to the formation of ultrafine magnetic Fe–Si nanograins embedded in the amorphous matrix [1–3]. Magnetic softness of the alloy is directly related to its ultrafine structure and explained in terms of the random anisotropy model [4]. The role of both Cu and Nb in the formation of such nanostructure is also very important. Cu segregates at the initial stage of crystallization to form Cu-rich clusters that multiply nucleation of Fe–Si grains. Rejection of insoluble and slow diffusing Nb atoms to the grain interfaces hinders the grain growth, which leads to the maintaining of a small mean grain size and decreasing of crystallization kinetics [5–7].

Crystallization kinetics in amorphous alloys and especially in the alloys that form a two-phase nanocrystal-amorphous structure is a key subject that provide new opportunities to design the desired structure and properties [8,9]. Generally two types of procedures could be used for kinetic studies. In some methods, estimated kinetic data fit to a theoretical reaction model. Using these so-called model-fitting methods, highly inaccurate activation energy and other kinetic parameters may be obtained [10]. In some other methods, there is no need to assume a reaction model for evaluation of kinetic data. According to these model-free or isoconversional methods, activation energy as a function of conversion extent could be acquired and used for kinetic investigations [11,12].

Nanocrystallization kinetics of Finemet type alloys are almost always investigated assuming the well-known Johnson–Mehl–Avrami (JMA) or similar kinetic models [13–15]. But continuous and isothermal DSC measurements, X-ray diffractometry, electron microscopy and Mössbauer kinetic analyses [16–19] show that such model-fitting methods cannot fit the experimental data. For example, quiet different values of the apparent activation energies from 143 to 567 kJ mol^{-1} obtained for the main transformation [19–24], indicating the problems associated with using of model-fitting methods. These problems are mainly due to inability of these

* Corresponding author. Tel.: +98 21 66165258; fax: +98 21 66005717.
E-mail address: madaah@sharif.edu (H.R.M. Hosseini).

0040-6031/$ – see front matter © 2009 Elsevier B.V. All rights reserved.
doi:10.1016/j.tca.2009.04.020

methods to distinguish the reaction complexity that occurs during the nanocrystallization of Finemet alloy [25,26]. In such cases, isoconversional methods could be used for the detection of reaction complexity. A large number of isoconversional methods have been conducted on polymer materials and metallic glasses [27–29]. The present study aims to use an advanced isoconversional method proposed by Vyazovkin [30–32] for calculating kinetic parameters of main transformation in Finemet alloy. To our knowledge, there are no pervious results in the literature about using this advanced isoconversional method for Finemet type alloys.

2. Experimental

2.1. Materials and methods

Ingot of $Fe_{73.5}Si_{13.5}B_9Cu_1Nb_3$ (at.%) alloy was prepared by arc melting under argon atmosphere using highly pure metals. Amorphous ribbons with a cross-section of 0.02 mm × 1.00 mm were prepared by melt spinning under protective argon atmosphere. The actual composition of the amorphous ribbons was determined by inductively coupled plasma (ICP) analysis. The amorphous nature of the ribbons was analyzed using X-ray diffraction with Co Kα (1.78897 Å) radiation. In order to investigate the structural transformations by X-ray diffraction, the samples of amorphous alloy were annealed at different temperatures (200, 300, 400, 500, 600 and 700 °C) for 1 h. To prevent oxidation during the heat treatment, the samples were sealed in quartz ampoules after repeated evacuation sequences. The magnetic properties were measured at room temperature using a vibrating sample magnetometer (VSM). The nanocrystallization kinetics was investigated with a Mettler Toledo DSC-1 instrument using a continuous heating regime with the heating rates, β, of 5–80 °C min^{-1}. The temperature (error less than 0.05%) and the enthalpy (error less than 1%) axes were calibrated using indium and zinc standards for all the heating rates. In this case, the samples weighing 20 mg were placed in standard platinum pans and heated in the DSC cell starting from the room temperature up to 700 °C under a stream of nitrogen with the 20 mL min^{-1} flow rate.

2.2. Kinetics study

It is well known that the transformation rate of a solid-state reaction in isothermal conditions is the product of two functions [33]:

$$\frac{d\alpha}{dt} = k(T)f(\alpha), \tag{1}$$

where $k(T)$ is the reaction rate constant, $f(\alpha)$ is the reaction model and α is the conversion fraction. For kinetic investigations, non-isothermal thermo-analytical techniques with a constant heating rate of $\beta = dT/dt$ are most commonly preferred techniques due to their several advantages such as rapidity and extended temperature range of measurements [34]. Accordingly, considering the Arrhenius form of the reaction rate constant, Eq. (1) may be rewritten as:

$$\frac{d\alpha}{dT} = \frac{A}{\beta}\exp\left(-\frac{E}{RT}\right)f(\alpha), \tag{2}$$

where A (s^{-1}) is the pre-exponential (frequency) factor, E is the activation energy and R is the universal gas constant.

Integration of Eq. (2) results in:

$$g(\alpha) \equiv \int_0^{\alpha}\frac{d\alpha}{f(\alpha)} = \frac{A}{\beta}\int_0^{T_\alpha}\exp\left(-\frac{E}{RT}\right)dT = \frac{A}{\beta}I(E,T), \tag{3}$$

where $g(\alpha)$ is the integral form of the reaction model and $I(E,T)$ is the temperature integral that does not have an analytical solution. Several approximations and numerical integration procedures such as Doyle [35], Kissinger–Akahira–Sunose (KSA) [36], Flynn–Wall–Ozawa (FWO) [37,38], Tang et al. [39], Coats and Redfern [40] and Starink [41,42] have been used to solve the temperature integral. For extracting more accurate information, Vyazovkin [30–32] developed an advanced isoconversional method that utilizes an accurate numerical integration. According to this method under non-isothermal condition, for each value of α, the activation energy is found by minimizing the following function:

$$\Phi(E_\alpha) = \sum_{i=1}^{n}\sum_{j\neq i}^{n}\frac{I(E_\alpha, T_{\alpha,i})\beta_j}{I(E_\alpha, T_{\alpha,j})\beta_i}, \tag{4}$$

and the temperature integral over small temperature segments is calculated as:

$$I(E,T) = \int_{T\alpha-\Delta\alpha}^{T\alpha}\exp\left(-\frac{E}{RT}\right)dT, \tag{5}$$

It is worth noting that in simpler methods, assuming a constant value of $E(\alpha)$ for this integration causes a systematic error as large as 20–30% in the value of $E(\alpha)$ that does not appear in the advanced integration method of Vyazovkin [43].

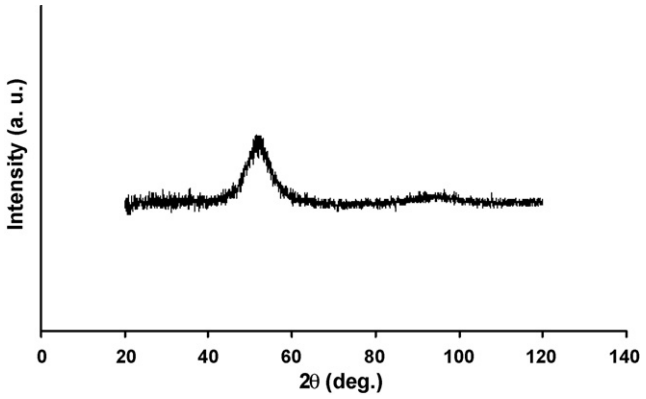

Fig. 1. X-ray diffraction pattern of amorphous $Fe_{73.5}Si_{13.5}B_9Cu_1Nb_3$ (at.%).

3. Results and discussion

X-ray diffraction pattern of the as quenched sample in Fig. 1 shows only a broad halo peak, which is a characteristic of amorphous state. The room temperature hysteresis loop of this sample

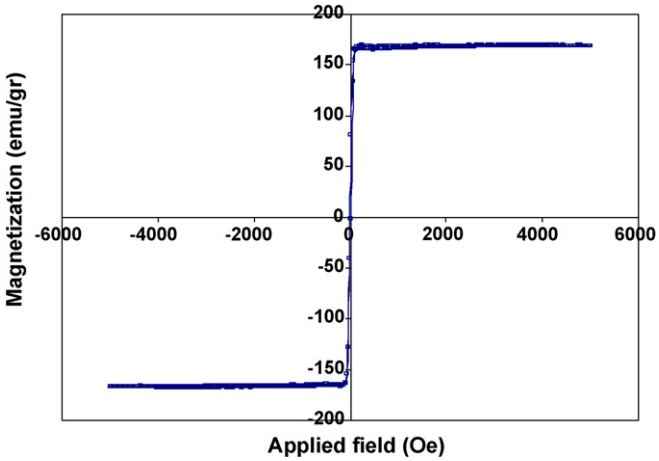

Fig. 2. Room temperature hysteresis loop of amorphous ribbon.

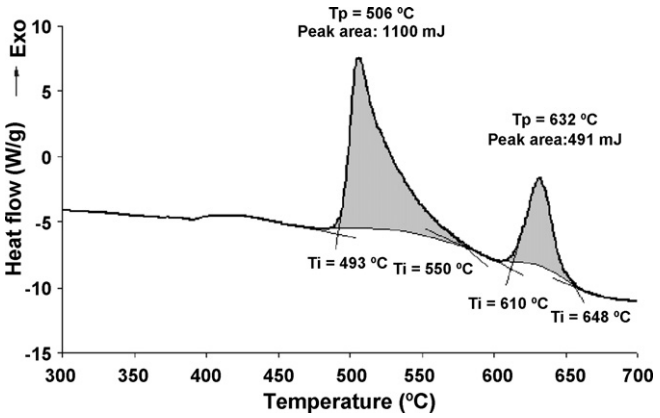

Fig. 3. DSC curve of the amorphous sample obtained during the heating cycle at the heating rate of 20 K min^{-1}.

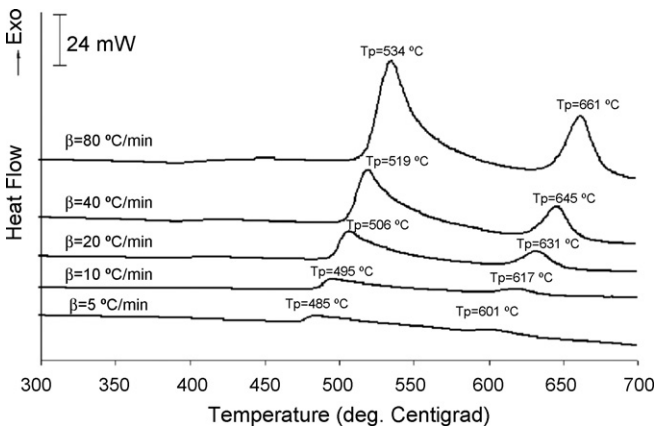

Fig. 5. DSC curves of the amorphous sample at various heating rates.

before any heat treatment in Fig. 2 shows the typical features of a soft magnetic material.

A typical DSC curve obtained during heating cycle of as quenched sample is presented in Fig. 3, which involves two exothermal peaks. The first peak corresponds to crystallization of Fe–Si nanograins and the second is related to the formation of boride phases. The small broad exothermic peak next to the primary crystallization peak probably corresponds to Cu clustering, which occurs before nanocrystallization. The crystallization onset temperature (T_i), peak temperature (T_p), endset temperature (T_f) and heat of reaction (the area under peak) for both peaks were determined on the DSC curve. The area under peak is directly related to the conversion fraction that is used for calculation of conversion versus temperature.

Isothermal structural changes of the samples could be found by X-ray diffraction patterns (Fig. 4). As could be seen, diffraction patterns of the samples annealed up to 400 °C contain the same halo peak, indicating an amorphous structure. Increase of annealing temperature reveals a sharp peak at $2\theta = 52.7°$ whose height increases with the increase of annealing temperature. This shows that at temperatures above 500 °C, nanocrystallization starts to occur and further increasing of annealing temperature to about 700 °C, leads to the formation of boride phases. These results are consistent with the DSC results (Fig. 3). The average crystallite size of the Fe–Si grains was calculated from the full-width at half-maximum of the (1 1 0) reflection using the Scherrer formula to be 14 and 19 nm for samples annealed at 500 and 600 °C, respectively.

For calculation of the kinetic parameters, multiple DSC scans (at least three scans) are needed. Fig. 5 shows the DSC curves of the amorphous samples taken at five various heating rates. The results showed that with increasing of heating rate, all values of the onset (T_i), peak (T_p) and endset (T_f) temperatures for both exothermic peaks shift to higher values, due to the presence of kinetic effects during the nanocrystallization process. There is a linear relation between these temperatures and logarithm of the heating rate as shown in Fig. 6.

Using DSC results, the activation energy of nanocrystallization process was calculated according to Vyazovkin, Kissinger [44] and also KSA, FWO, Tang and Starink methods for comparison. According to Kissinger method, which is widely used for the calculation of activation energy in Finemet type alloys [45–47], a single value of $E = 270 \pm 10$ kJ mol^{-1} was obtained from the slop of Kissinger relation:

$$\ln \frac{\beta_i}{T_{p,i}^2} = \text{Const}\left(-\frac{E}{RT_{p,i}}\right), \tag{6}$$

Activation energy is generally defined as the threshold value of energy above which the fluctuation of energy is sufficient for the elementary reaction to occur, and it should have a characteristic and constant value for each particular reaction [26]. But for nanocrystallization of amorphous Finemet alloy, the activation energy belongs to several atoms (Fe, Si, B, Nb and Cu), and also the process of nucleation and growth occurs under continuously varied chemical composition. Obviously, for such complex crystallization process, activation energy could not have a single value and the

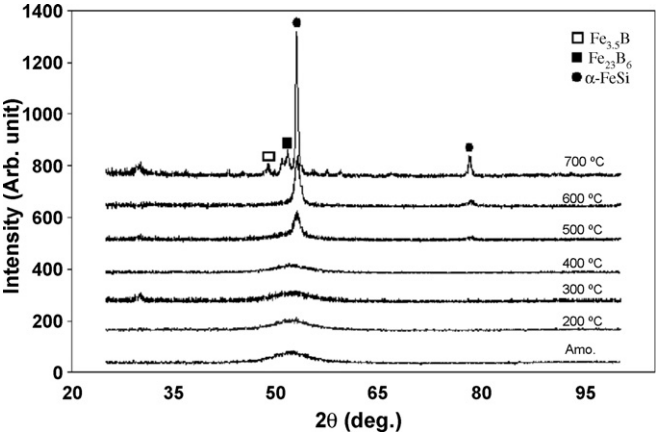

Fig. 4. X-ray diffraction patterns of the samples isothermally annealed at various temperatures.

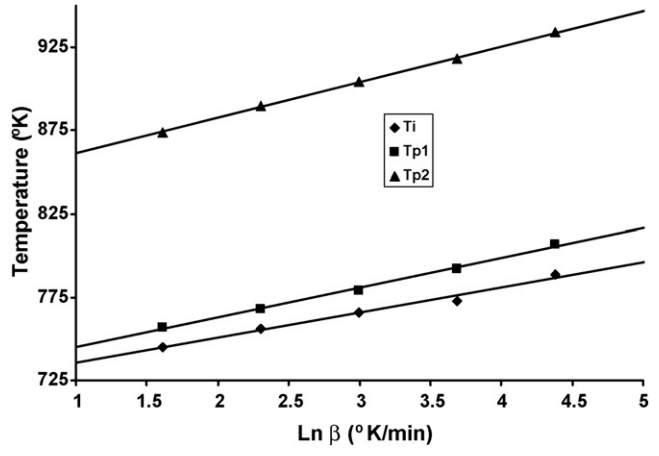

Fig. 6. Plot of the characteristic temperatures versus logarithm of the heating rates for both exothermic peaks.

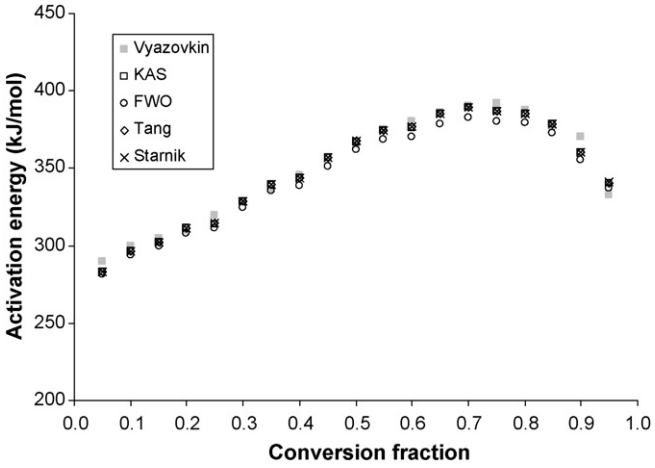

Fig. 7. Activation energy versus conversion extent.

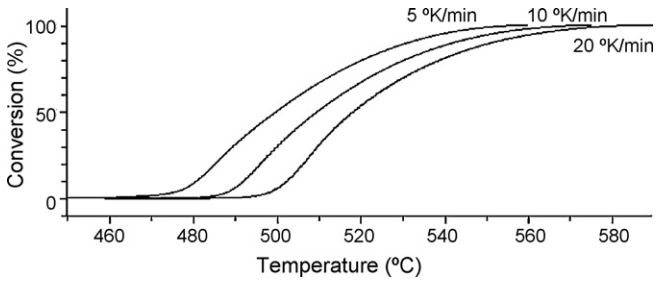

Fig. 8. Plot of conversion extent versus temperature for the heating rates of 5, 10 and 20 K min^{-1}.

above-mentioned constant value obtained from Kissinger method could not be acceptable.

So, variable activation energy versus conversion according to Vyazovkin advanced isoconversional method was calculated, which is shown in Fig. 7, where three regions are noticeable; first, an increase of $E(\alpha)$ with α occurred corresponding to the initial stage of crystallization ($\alpha < 0.1$) that reached up to 300 kJ mol^{-1} for $\alpha = 0.1$. For volume fraction in the range of 0.1–0.75, activation energy increased approximately linearly, with the mean value of 350 kJ mol^{-1}. At the final stage of crystallization (0.75–1), activation energy decreased sharply. The results showed that the mean value of activation energy from the Vyazovkin method (350 kJ mol^{-1}) was higher than the one obtained from the Kissinger method (270 ± 10 kJ mol^{-1}) in the same experiments, showing inaccuracy of the Kissinger method. As could be seen in Fig. 7 isoconversional methods such as KSA, FWO, Tang and Starink show similar results (error less than 1%). These results, as anticipated, show that the nanocrystallization in Finemet alloy is a complex and multi-step reaction. At the initial stages where nucleation is dominated, the local activation energy has its lowest value. At this stage, precipitation of Cu-rich clusters is supposed to provide a high number density of nucleation sites, due to higher Fe concentration in their vicinity [4] and also due to the heterogeneous nucleation promoted by lower interface energy [6]. Since the solubility of copper in Fe-based matrix is very low, heterogeneous nucleation needs much lower energy compared to the homogeneous one, and the amorphous glassy precursor has metastable nature, then the nucleation process and its sub-processes may occur quickly or even during solidification. Indeed, the lower effective activation energy in the initial stage of primary crystallization seems mainly attributed to the presence of quenched-in nuclei (embryos) that is due to finite cooling rate during glass formation [48,49]. In the middle stages ($\alpha = 0.1$–0.75), as the Fe–Si phase forms, Nb and B atoms are excluded from the FeSi crystallites (because of their low solubility) and enriched in grain interfaces. Slow diffusion of Nb atoms forms a Nb-rich shell and acts as a diffusion barrier that gradually hinders further growth. Increase of activation energy at this stage could be related to the continuous variation of chemical composition during the conversion and also contribution of several atoms in the nanocrystallization process. Diffusion has also an important role in this stage and the overall process rate becomes dependent on the diffusion rate of the atoms as well as on the chemical reaction rate. Additionally, the kinetic parameters such as diffusion coefficient are composition-dependent and will change as the crystallization proceeds [16]. Finally, the abrupt decrease of $E(\alpha)$ at the end of the transformation may be as a result of inaccurate base line subtraction. Also it must be noted that after 0.8 conversions, the amorphous matrix is enriched by Nb and B atoms. Thus further growth is almost impossible and so in our opinion, activation energy for this stage has no physical meaning. The remained amorphous phase transforms into boride phases at higher temperatures.

Controversial results related to the activation energy of Finemt alloys have been reported. Differences in results are probably due to nanocrystallization complexity of the Finemet alloy, initial condition of amorphous precursor and also the precision of used kinetics methods. Lu et al. [25,26] have found the activation energy to be equal to 386 ± 30 kJ mol^{-1} using the isoconversional methods. Isothermal studies by Zhou et al. [50] showed the activation energy equals to 370 kJ mol^{-1}. Using Kissinger model-fitting method, Phan et al. [22] and Illekova et al. [20] have found the activation energy values of 313 and 418 ± 8 kJ mol^{-1}, respectively. The mean value of this parameter obtained in this study (350 kJ mol^{-1}) seems to be comparable with those obtained by Lu et al. and Zhou et al. and relative differences could be attributed to the precursor condition and the precision of used method.

The plots of conversion fraction versus temperature corresponding to $\beta = 5$, 10 and 20 K min^{-1} are shown in Fig. 8. The volume fraction crystallized at any temperature is given as $\alpha = S_T/S$, where S is the total area under exothermic peak and S_T is the area between the initial and the selected temperatures [51]. The sigmoid shape of the fractional conversion curves shown in Fig. 8 indicates a slow initial period ($\alpha < 0.1$) corresponding to nucleation that occurs at various points in the bulk of the sample. The middle stage ($0.1 < \alpha < 0.75$) shows the growth of nuclei, already formed at the initial stages. The Nb diffusion barrier that is gradually formed at this stage inhibits further growth and affects the shape of the conversion-temperature plot. The final decay part ($\alpha > 0.75$) is the consequence of attaching of the nuclei or diffusion field around them.

Additionally, with an Arrhenius temperature dependence, the volume fraction crystallized under the non-isothermal conditions could be expressed as [52]:

$$\alpha = 1 - \exp\left(-Q\left(\frac{K_V T^2}{\beta}\right)^n\right), \tag{7}$$

where Q is a parameter equal to $gR(R/E_G)^m \sum_{s=0}^{m} (-1)^s \binom{m}{s} (E_N + sE_G)^{-1}$ and K_V is reaction rate constant:

$$K_V = (I_{V0} u_0^m)^{(1/n)} \exp\left(-\frac{E}{RT}\right), \tag{8}$$

where n and m are important kinetic parameters that supply information about the reaction mechanism and the dimensionality of crystal growth, respectively [53,54]. The crystallization exponent, n, related to the number of growth dimension, m, and to the number

Table 1
Maximum crystallization rate and kinetic exponent, n, for nanocrystallization in Finemet alloy.

B (K min^{-1})	10^3 $(dx/dt)_{\|P}$ (s^{-1})	n
5	2.7	1.39
10	5.3	1.4
20	10.3	1.4
40	20	1.41
80	39.2	1.43

of nuclei forming stages, s [55]:

$$n = m + s, \tag{9}$$

where $s = 0$ is for instantaneous nucleation and $s = 1$ is for constant nucleation rate.

It is possible to calculate the kinetic exponent, n, using the experimental data on T_p and $(dx/dt)_{|P}$, according to the following equation [56,57]:

$$n = RT_P^2 \left(\frac{dx}{dt}\right)_{|P} (0.37\,\beta E)^{-1}, \tag{10}$$

where $(dx/dt)_{|P}$ is maximum crystallization rate for each heating rate. Using a set of exotherms taken at different heating rates, the values of n and $(dx/dt)_{|P}$ were acquired (Table 1). The mean value of n could be assumed as the most probable value and used for recognition of reaction mechanism and dimensionality of crystal growth. Considering the site saturation condition ($s = 0$), the mean value of kinetic exponent, $n = 1.44 \pm 0.05$, is relatively consistent with one-dimensional growth mechanism. Lu et al. [25,26] have found that the values of n lie between 1 and 2 in a wide rang of $0.2 < \alpha < 0.9$ and concluded that one-dimensional growth at a near zero nucleation rate surface crystallization is dominant mechanism. By obtaining n values as a function of conversions, Zhou et al. [50] have also found the same values of n between 1 and 2 for $0.2 < \alpha < 0.9$. In another study, Conde et al. [58,59] have obtained n values near 1 for Finemet alloys and implied similar analysis about reaction mechanism. Comparison of the kinetic exponent obtained here shows good concurrence with above-mentioned results.

However, the activation energy has more important role compared to pre-exponential factor, A, and reaction model, $f(\alpha)$, for kinetic study. Anyway knowing all kinetic triplets are necessary for a complete kinetic study. In order to do a detailed study on crystallization kinetics and distinguish which one of the listed models in Table 2 can describe the nanocrystallization process in Finemet alloy, integral form of the reaction model, $g(\alpha)$, was calculated numerically. To determine $g(\alpha)$, Eq. (3) was used and the pre-exponential factor was evaluated using the compensating correlation of E and A as [43,60]:

$$\log A_i = aE_i - b, \tag{11}$$

where a and b are constants and A_i and E_i are Arrhenius parameters associated with a particular reaction model, $g_i(\alpha)$, in Table 2. Accordingly, the values of a and b were obtained as 6.69×10^{-5} and 0.875, respectively.

The numerically reconstructed form of experimental kinetics model, $g(\alpha)$, corresponding to different heating rates and also some theoretical models from Table 2 are shown in Fig. 9. Comparison of the experimental and theoretical models (solid line) clearly shows the mechanism changes during the transformation. The results showed that selected heating rates did not change the mechanism of reaction and the experimental data at the selected heating rates are approximately identical. As shown in Fig. 9, no single model from Table 2 could perfectly fit the numerical values of $g(\alpha)$, and the mechanism of transformation changes with conversion progress. Nevertheless it could be seen that nanocrystallization almost follows the one-dimensional diffusion mechanism (16 in the diagram).

Table 2
Common solid-state reaction models used to describe the crystallization process and the corresponding values of A and E.

i	Reaction model	$g(\alpha)$	E (kJ/mol)	A (min^{-1})
1	Power low, $n = 1/4$	$\alpha^{1/4}$	45	9.84E1
2	Power low, $n = 1/3$	$\alpha^{1/3}$	64	2.30E2
3	Power low, $n = 1/2$	$\alpha^{1/2}$	102	1.06E6
4	Power low, $n = 3/2$	$\alpha^{3/2}$	328	2.08E21
5	Avrami–Erofeev, $n = 1.5$	$[-\ln(1-\alpha)]^{2/3}$	206	2.06E13
6	Avrami–Erofeev, $n = 2$	$[-\ln(1-\alpha)]^{1/2}$	152	4.03E8
7	Avrami–Erofeev, $n = 3$	$[-\ln(1-\alpha)]^{1/3}$	97	5.94E5
8	Avrami–Erofeev, $n = 4$	$[-\ln(1-\alpha)]^{1/4}$	70	7.22E3
9	Three-dimensional phase boundary reaction	$1-(1-\alpha)^{1/3}$	280	6.48E17
10	Two-dimensional phase boundary reaction	$1-(1-\alpha)^{1/2}$	261	4.59E16
11	One-dimensional phase boundary reaction	α	215	9.04E13
12	Second order reaction	$(1-\alpha)^{-1}-1$	442	3.46E29
13	First order reaction	$-\ln(1-\alpha)$	315	5.38E20
14	Three-dimensional diffusion	$[1-(1-\alpha)^{1/3}]^2$	572	9.22E36
15	Two-dimensional diffusion	$(1-\alpha)\ln(1-\alpha)+\alpha$	502	6.01E32
16	One-dimensional diffusion	α^2	443	9.71E27

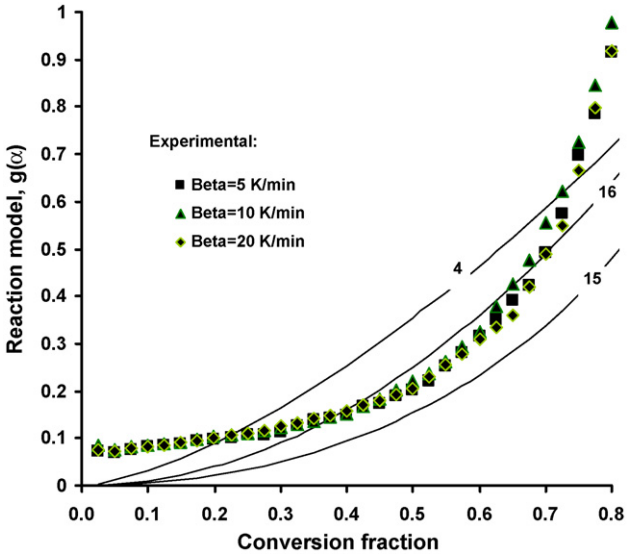

Fig. 9. Variation of the integral form of the reaction model, $g(\alpha)$, versus conversion and also some theoretical models listed in Table 2.

Mechanism changes or deviations from a selected model may be related to the relative contribution of nucleation and crystal growth through the process and role of diffusion of various atoms. At initial stage of crystallization, contribution of nucleation is more than growth process and this may be the reason for deviation of process from the considered mechanism. Deviation of $g(\alpha)$ at the final stage of crystallization, as mentioned above, is attributed to the abrupt decrease of $E(\alpha)$. At this stage, amorphous matrix is fully enriched by Nb and B, and further growth is almost impossible, so the kinetics data at this stage are not helpful for the main transformation investigations.

4. Conclusions

Isoconversional kinetics of nanocrystallization in Finemet alloy was investigated according to the Vyazovkin method. The

activation energy as a function of conversion was calculated and found to vary with conversion extent, indicating a reaction complexity. Changes in activation energy during nanocrystallization reflect mechanism changing during the reaction, which could not be distinguished with the model-fitting procedures such as Kissinger method. In order to distinguish how and when the mechanism of process changes, numerical reconstruction of the reaction model using experimental data was performed. The results showed that nanocrystallization mechanism could not perfectly fit on a single theoretical model. Nevertheless nanocrystallization in Finemet alloy relatively follows one-dimensional diffusion mechanism.

Acknowledgements

The authors are grateful to the Parsel Company (Mettler Toledo representative) and Mr. Ali sanei for their technical supports.

References

[1] M. Sakurai, M. Matsuura, S.H. Kim, Y. Yoshizawa, K. Yamauchi, K. Suzuki, Mater. Sci. Eng. A 179–180 (1994) 469.
[2] G. Herzer, J. Magn. Magn. Mater. 157–158 (1996) 133.
[3] M.E. McHenry, M.A. Willard, D.E. Laughlin, Prog. Mater. Sci. 44 (1999) 291.
[4] G. Herzer, IEEE Trans. Magn. 26 (1990) 1397.
[5] K. Hono, K. Hiraga, Q. Wang, A. Inoue, T. Sakman, Acta Metall. Mater. 40 (1992) 2137.
[6] G. Herzer, in: K.H.J. Buschow (Ed.), Handbook of Magnetic Materials, vol. 10, Elsevier, Amsterdam, 1997, pp. 415–462.
[7] C.F. Barbatti, E.H.C.P. Sinnecker, R.S. Sarthour, A.P. Guimarães, J. Alloys Compd. 369 (2004) 136.
[8] M.T. Clavaguera-Mora, N. Clavaguera, D. Crespo, T. Pradell, Prog. Mater. Sci. 47 (2002) 559.
[9] D.M. Minic, A. Maricic, B. Adnadevic, J. Alloys Compd. 473 (2009) 363.
[10] S. Vyazovkin, C.A. Wight, Thermochim. Acta 340/341 (1999) 53.
[11] S. Vyazovkin, Int. J. Chem. Kinet. 28 (1996) 95.
[12] N. Sbirrazzuoli, L. Vincent, S. Vyazovkin, Chemometr. Intell. Lab. Syst. 54 (2000) 53.
[13] M.E. McHenry, F. Johnson, H. Okumura, T. Ohkubo, V.R.V. Ramanan, D.E. Laughlin, Scripta Mater. 48 (7) (2003) 881.
[14] D. Crespo, T. Pradell, M.T. Clavaguera-Mora, N. Clavaguera, Phys. Rev. B 55 (1997) 3435.
[15] J.M. Barandiaran, I. Teller, J.S. Garitaonandia, H.A. Davies, J. Non-Cryst. Solids 329 (2003) 57.
[16] E. Illekova, Thermochim. Acta 387 (2002) 47.
[17] G. Hampel, A. Pundt, J. Hesse, J. Phys.: Condens. Matter 4 (1992) 3195.
[18] N. Le caude, J.C. Perron, J. Magn. Magn. Mater. 160 (1996) 263.
[19] A. Cserei, J. Jiang, F. Aubertin, U. Gonser, J. Mater. Sci. 29 (1994) 1213.
[20] E. Illekova, K. Czomorova, F.A. Kuhnast, J.M. Fiorani, Mater. Sci. Eng. A 205 (1996) 166.
[21] S.D. Kaloshkin, I.A. Tomilin, Thermochim. Acta 280–281 (1996) 303.
[22] M.H. Phan, H.X. Peng, M.R. Wisnom, S.C. Yu, N.D. Tho, N. Chau, Composites Part A 37 (2006) 191.
[23] W.Z. Chen, P.L. Ryder, Mater. Sci. Eng. B 34 (1995) 204.
[24] C. Li, X. Tian, X. Chen, A.G. Ilinsky, L. Shi, Mater. Lett. 60 (2006) 309.
[25] W. Lu, L. Yang, B. Yan, W. Huanga, J. Alloys Compd. 420 (2006) 186.
[26] W. Lu, B. Yan, W. Huang, J. Non-Cryst. Solids 351 (2005) 3320.
[27] P. Simon, E. Illekova, S.C. Mojumdar, J. Thermal. Anal. Calorim. 83 (2006) 67–69.
[28] K.N. Lad, R.T. Savalia, A. Pratap, G.K. Dey, S. Banerjee, Thermochim. Acta 473 (2008) 74–80.
[29] A. Pratap, T.L.S. Rao, K.N. Lad, H.D. Dhurandhar, J. Thermal. Anal. Calorim. 89 (2007) 399–405.
[30] S. Vyazovkin, D. Dollimore, J. Chem. Inf. Comp. Sci. 36 (1996) 42.
[31] S. Vyazovkin, J. Comput. Chem. 22 (2001) 178.
[32] S. Vyazovkin, J. Comput. Chem. 18 (1997) 393.
[33] S. Vyazovkin, Thermochim. Acta 355 (2000) 155.
[34] K. Song, X. Bian, J. Gu, X. Li, M. Xie, C. Dong, J. Alloys Compd. 465 (2008) L7–L13.
[35] C.D. Doyle, J. Appl. Polym. Sci. 6 (1962) 639.
[36] T. Akahira, T. Sunose, Res. Rep. Chiba Inst. Technol. 16 (1971) 22.
[37] J.H. Flynn, L.A. Wall, J. Res. Natl. Bur. Stand. Sect. A 70 (1966) 487.
[38] T. Ozawa, Bull. Chem. Soc. Jpn. 38 (1965) 1881.
[39] W. Tang, Y. Liu, H. Zhang, C. Wang, Thermochim. Acta 408 (2003) 39.
[40] A.W. Coats, J.P. Redfern, Nature 201 (1964) 68.
[41] M.J. Starink, Thermochim. Acta 404 (2003) 163.
[42] M.J. Starink, J. Mater. Sci. 42 (2007) 483.
[43] S. Vyazovkin, in: M.E. Brown, P.K. Gallagher (Eds.), Handbook of Thermal Analysis and Calorimetry, vol. 5, Elsevier B.V., 2008, pp. 503–538.
[44] H.E. Kissinger, Anal. Chem. 29 (1957) 1702.
[45] N. Bayri, T. Izgi, H. Gencer, P. Sovak, M. Gunes, S. Atalay, J. Non-Cryst. Solids 355 (2009) 12.
[46] N. Chau, N.Q. Ho, N.H. Luong, J. Magn. Magn. Mater. 290–291 (2005) 1547.
[47] N.Q. Hoa, N. Chau, S.C. Yu, T.M. Thang, N.D. The, N.D. Tho, Mater. Sci. Eng. A 449–451 (2007) 364.
[48] A. Gupta, M. Jayaraj, S. Lal, R. Verma, J. Phys. F: Met. Phys. 18 (1988) 2159–2169.
[49] D. Jacovkis, J. Rodriguez-Viejo, M.T. Clavaguera-Mora, J. Phys.: Condens. Matter 17 (2005) 4897–4910.
[50] F. Zhou, K. He, M. Sui, Mater. Sci. Eng. A 179–189 (1994) 1419.
[51] Z. Yuan, X. Chen, B. Wang, Y. Wang, J. Alloys Compd. 407 (2006) 163.
[52] J. Vazquez, C. Wagner, P. Villares, R. Jimenez-Garay, Acta Metall. 44 (1996) 4807.
[53] J. Vazquez, P.L. Lopez-Alemany, P. Villares, R. Jimenez-Garay, Mater. Lett. 35 (1998) 50.
[54] E.R. Shaaban, Physica B 373 (2006) 211.
[55] K. Matusita, S. Sakka, Phys. Chem. Glass 20 (1979) 81.
[56] J. Vazquez, P.L. Lopez-Alemany, P. Villares, R. Jimenez-Garay, J. Phys. Chem. Solids 61 (2000) 493.
[57] J. Vazquez, P.L. Lopez-Alemany, P. Villares, R. Jimenez-Garay, J. Alloys Compd. 270 (1998) 179.
[58] J.M. Borrego, C.F. Conde, M. Millán, A. Conde, M.J. Capitán, J.L. Joulaud, Nanostruct. Mater. 10 (1998) 275.
[59] C.F. Conde, A. Conde, Mater. Lett. 21 (1994) 409.
[60] A.A. Joraid, A.A. Abu-Sehly, M. Abu El-Oyoun, S.N. Alamri, Thermochim. Acta 470 (2008) 98.